Progress in Scatterometer Application

W. Timothy Liu*

*Jet Propulsion Laboratory, California Institute of Technology,
M.S. 300-323, 4800 Oak Grove Dr., Pasadena, CA 91109, U.S.A.*

Progress in the scientific application of space-based scatterometer data over the past two decades is reviewed. There has been continuous improvement in coverage, resolution, and accuracy. Besides the traditional applications in weather and ocean-atmosphere interaction, which are based on ocean surface wind vectors, emerging applications over land and ice are also described. Future missions and new technology are introduced.

1. Introduction

Ocean circulation is largely driven by wind. Prior to the advent of spaceborne scatterometer, almost all ocean wind measurements came from merchant ships. The distribution and quality of ship-based wind measurements are far from satisfactory. Today, operational numerical weather prediction (NWP) gives us a global wind field every six hours, but NWP depends on models, which are limited by our knowledge of the physical processes and the availability of data. Spaceborne microwave scatterometers are the only proven instruments that give us measurements of ocean surface wind vectors (both speed and direction) under clear and cloudy conditions, day and night. They give us not only a near-synoptic global view, but also a detail that cannot be achieved with NWP models. Such coverage and resolution are crucial to understanding and predicting changes in weather and climate. The past decade has seen continuous improvement to the coverage and resolution of ocean surface winds. Although the primary objective of scatterometry is to measure wind vectors over the ocean, new applications over ice and land have recently emerged.

This review of the scientific applications of a series of scatterometer missions is not intended to be exhaustive; rather, it represents the progress made in scientific applications in the past two decades. The scope of this paper does not allow a detailed review of the technique of wind retrievals from scatterometer data.

2. Principles of Scatterometry

During the Second World War, marine radar operators observed noises on their radar screens, which obscured small boats and low-flying aircraft. They termed this noise "sea clutter". This clutter was the backscatter of the radar pulses by the small waves on the ocean's surface (Moore and Fung, 1979). The radar operators at that time were quite annoyed by these noises, not knowing that, a few decades later, scientists would make important applications.

The scatterometer sends microwave pulses to the earth's surface and measures the power backscattered from the surface roughness. The roughness may describe the characteristics of polar ice or vegetation over land. Over the ocean, which covers over three-quarters of the earth's surface, the backscatter is largely due to the small centimeter waves on the surface. The idea of remote sensing of ocean surface winds was based on the belief that these surface ripples are in equilibrium with the local wind stress. Based on measurements in an aircraft experiment, Jones *et al*. (1978) confirmed that, at incident angles greater than 20°, the backscatter coefficient increases with wind speed. They also demonstrated the anisotropic characteristics of the scattering. The backscatter depends not only on the magnitude of the wind stress but also the wind direction relative to the direction of the radar beam (azimuth angle). The capability of measuring both wind speed and direction is the major, unique characteristic of the scatterometer.

Because the backscatter is symmetric about the mean wind direction, observations at many azimuth angles are needed to resolve the directional ambiguity. A

* E-mail address: liu@pacific.jpl.nasa.gov

scatterometer that measures only at two orthogonal azimuth angles, such as Seasat (see Section 3), will always includes wind solutions of nearly equal magnitude and 180° apart. To select wind direction from Seasat data, a subjective dealiasing technique was used by Wurtele *et al.* (1982), and objective dealiasing methods were used by Hoffman (1982) and Atlas *et al.* (1987). Because of the uncertainties in the wind retrieval algorithm and noise in the backscatter measurements, the problem with directional ambiguity was not entirely eliminated with additional azimuthal looks in the scatterometers launched after Seasat. A median filter iteration technique initialized by the wind direction solution closest to NWP wind field has been commonly used to remove the directional ambiguity (e.g., Shaffer *et al.*, 1991; Gonzales and Long, 1999).

There is a long history of theoretical studies of the relationship between wind and backscatter (e.g., Wright, 1968; Plant, 1986; Donelan and Pierson, 1987), based on laboratory data. However, these theoretical or dynamic-based relationships (geophysical model functions, GMF) were not sufficient for operational wind retrieval in open oceans. The GMF, from which ocean surface wind vectors are retrieved from the observed backscatter, is largely based on empirical fits of data (e.g., Jones *et al.*, 1978; Freilich and Dunbar, 1993; Thiria *et al.*, 1993; Stoffelen and Anderson, 1997; Wentz and Smith, 1999).

Because the capillary waves, which determine backscatter, are governed by stress, the approach of relating backscatter observations directly to measurements of surface stress have been made by Liu and Large (1981), Weissman and Graber (1999), and others. The definition of the geophysical data product of scatterometer as the equivalent neutral wind (Liu and Tang, 1996) is based on the same reasoning (see Subsection 5.3 for further discussion). Brown (2000) also presented an algorithm that relates the backscatter to pressure gradient or geostrophic winds, which may be more coherent over the scatterometer footprint than surface winds.

3. Scatterometer Missions

Historically, scatterometers of the European Space Agency (ESA) used the C-band (5 GHz), but the National Aeronautics and Space Administration (NASA) prefers the Ku-band (14 GHz). Shorter ocean surface waves have stronger influence on backscatter at higher frequencies. The Ku-band is more sensitive to wind variation at low winds but is more subjective to rain contamination. Five scatterometers have been launched on polar-orbiting satellites and their major characteristics are summarized in Fig. 1.

NASA launched a scatterometer on the Seasat Mission in June 1978. Four fan-beam, dual-polarized antennas, oriented at 45° and 135° to the spacecraft subtrack, illuminated two 500-km swaths, one on each side of the spacecraft, providing wind vectors at 50-km resolution. However, only one side was in operation most of the time, covering less than 40% of the global ocean daily. The incident angle varies from 25° to 55°. The accuracy of the backscatter is about 0.7 db. The two orthogonal azi-

Spaceborne Scatterometers
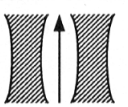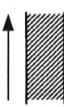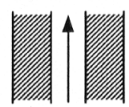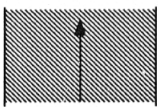
	SEASAT	ERS-1/2	NSCAT	QuikSCAT
Frequency	14.6 GHz	5.3 GHz	13.995 GHz	13.402 GHz
Scan Pattern				
Polarization	V-H, V-H	V ONLY	V, V-H, V	V, H
Inc. Angle	22°-55°	18°-47°, 24°-57°	18°-57°, 22°-63°	46°, 54°
Beam Resolution	Fixed Doppler	RANGE GATE	Variable Doppler	Spot
Resolution	50 km	50 km	25 km	25 km
Swath	500 km 500 km	500 km	600 km 600 km	1800 km
Daily Coverage	Variable	41%	77%	93%
Dates	6/78 – 10/78	8/91-1/01	8/96 – 6/97	6/99 +

Fig. 1. Characteristics of spaceborne scatterometers.

muth angles were not able to resolve the wind direction unambiguously. Seasat failed in October 1978.

A scatterometer was launched by ESA on the first European Remote Sensing (ERS-1) Satellite in August, 1991, and it was followed by an identical instrument on the ERS-2, which was launched in April 1995 and put into operation in 1996. The ERS scatterometers scan a 500-km swath on one side of the satellite, and measure at three azimuth angles, 45°, 90°, and 115°, with vertical polarization only. They provided winds over only 41% of the global ocean daily. The incident angle varies from 22° to 59° for the fore and aft beams and from 18° to 51° for the mid-beam. The backscatters have 50-km spatial resolution but are sampled at 25 km.

The NASA Scatterometer (NSCAT) was launched in August 1996 on the first Japanese Advanced Earth Observing Satellite (ADEOS), which was later renamed Midori. The six fan-beam antennas provide 600-km swaths on both sides of the spacecraft, covering 77% of the global ocean at 25-km resolution daily. The accuracy of backscatter is 0.2 db. The antennas made observations at 45°, 115°, and 135° azimuth angles. The fore and aft beams measure only at vertical polarization, with incident angle varies from 22° to 63°, while the midbeam measures at both vertical and horizontal polarization with incident angle varies from 18° to 51°. The unexpected destruction of the solar array caused the early demise of NSCAT, after it had returned nine months of data.

NASA launched QuikSCAT, a Ku-band scatterometer with a new design, in 1999. It uses pencil-beam antennas in a conical scan and has a continuous 1,800-km swath that covers 93% of the global ocean in a single day. The standard wind product has 25-km spatial resolution, but special products with 12.5-km resolution have been produced for selected regions (further discussion in Subsection 4.3). It measures horizontally and vertically polarized backscatter at 46° and 54° incident angles respectively.

4. Accuracy

4.1 Moderate conditions

Seasat wind vectors were found to meet instrument specifications in a number of studies (e.g., Jones *et al.*, 1982; Schroeder *et al.*, 1982; Brown, 1982). Bentamy *et al.* (1998) found good agreement between the interpolated wind fields derived from ERS-1 data and weekly and monthly averaged NWP wind fields. Ebuchi and Graber (1998) examined the distribution of wind direction derived from ERS scatterometers. The quality of NSCAT winds was shown to be above expectation through comparison with *in situ* measurements (e.g., Bourassa *et al.*, 1997; Freilich and Dunbar, 1999), and through comparison with winds from the analysis of NWP models (e.g.,

Liu *et al.*, 1998b; Atlas *et al.*, 1999; Ebuchi, 1999).

In examining over 5000 collocated QuikSCAT and buoy measurements, Wentz *et al.* (2001) found that there is almost no mean difference (bias) in wind speed and only 6° in wind direction. The root-mean-square differences are 0.7 m/s and 13°. The accuracy of QuikSCAT wind measurements exceeds instrument specification, and is better than NSCAT.

4.2 Extreme conditions

Theoretical studies (e.g., Donelan and Pierson, 1987) suggest a low-wind cut-off and high-wind saturation in deriving winds from backscatter. Such limitations have not been clearly observed. The accuracy of wind retrieval under weak winds (<3 m/s), strong winds (>15 m/s), and high precipitation is uncertain because of the lack of *in situ* standards for validation. Austin and Pierson (1999) expounded the difficulty of finding appropriate standards for validation under extreme conditions. Plant (2000), using NSCAT data, showed that the low-wind cut-off is lower than predicted, and the accuracy at low wind speeds depends on the variability of winds within the footprint. There are clear indications that rain affects wind retrieval but there is no indication of the level of rain at which wind retrieval becomes invalid using existing algorithms. Useful information will be lost if all winds retrieved under rainy conditions are discarded.

There is a great deal of interest in the feasibility of using scatterometers to measure the strong winds in tropical cyclones (TC). Quilfen *et al.* (1998), using ERS data, demonstrated the potential of scatterometer winds in monitoring TCs, but indicated that the coarse resolution of ERS scatterometers limited their usefulness. Jones *et al.* (1999) showed that the NSCAT algorithm underestimates wind speed in TCs and proposed a new method of wind retrieval. Donnelly *et al.* (1999), using measurements by scatterometers on aircraft, also exposed the deficiencies of existing scatterometer algorithms for high winds.

When the backscatter coefficients in dB (logarithmic scale) are plotted against wind speed, the curve becomes flat at wind speeds above 20 m/s. The results appear to support the theoretical postulation of backscatter saturation at high winds. However, sensitivity can still be observed in linear plots. In a similar aircraft experiment, Yueh *et al.* (2000) demonstrated that horizontal polarization is more sensitive than vertical polarization at high winds; there was still significant variation of backscatter as a function of wind at wind speeds higher than 35 m/s. Wentz *et al.* (2001) showed that the backscatter measured by QuikSCAT is sensitive to wind variation at wind speeds as high as 50 m/s, under clear-sky conditions. Yueh *et al.* (2001) showed that the backscatter measured by QuikSCAT over TC is sensitive

to the variation of hurricane-scale (up to 50 m/s) winds at various rain rates.

4.3 With high spatial resolution

The current standard 25-km resolution wind product of QuikSCAT is derived from an ellipsoidal instantaneous antenna footprint with characteristic dimension of 25×35 km (so-called "egg"). Using onboard filtering, the egg can be divided into smaller, contiguous "slices" having characteristic dimensions of about 6×25 km (Spencer *et al.*, 2000). The computation of backscatter and wind from the slices will, in principle, provide higher spatial resolution. A limited amount of surface wind data at 12.5 km resolution has been produced from QuikSCAT and successfully applied in studies of tropical cyclones and coastal eddies (e.g., Liu *et al.*, 2001a).

Long *et al.* (1993) developed a technique to produce resolution-enhanced backscatter (with 8 km resolution) by combining multipass data, and successfully applied this to land and ice studies, when temporal resolution is not critical (see Subsections 8.2 and 8.3). The dense sampling in QuikSCAT slice data makes it possible to apply the resolution-enhancement technique to a single pass of data, thus increasing the spatial resolution of ocean surface winds without sacrificing the temporal resolution (David Long, personal communication, 2001). However, the amount of accuracy degradation, if any, caused by the gaining spatial resolution, in using slices, has not been adequately evaluated.

5. Secondary Factors

While wind is the primary factor in the changes of backscatter measured by a scatterometer, other secondary factors, such as sea surface temperature (SST) (Subsection 5.1), surface film (Subsection 5.2), atmospheric stability (Subsection 5.3), and surface current (Subsection 5.4) may also affect scatterometer measurement, and may cause errors in wind retrieval. With the increasing accuracy of scatterometer wind measurement, understanding and quantifying such effects is becoming increasingly important and have become scientific fields in their own right.

5.1 Sea surface temperature

SST may affect capillary waves and backscatter through viscosity (Lleonart and Blackman, 1980). Liu (1984) showed that the difference between collocated wind speed measured by Seasat scatterometer and buoys is a function of SST, particularly at low wind speeds (<6 m/s). The dependence was confirmed by Freilich (1986). Zheng *et al.* (1997a) found that wind errors have a much stronger dependence on SST, but with a trend opposite to those previously observed in the open ocean. Instead of examining wind errors, Ebuchi (1997) found that the backscatter measured by ERS scatterometers is a function of SST, but concluded that the dependence is not caused by the temperature dependence of viscosity or atmospheric stability.

5.2 Natural surfactants

The backscatter attenuation caused by accidental oil-spills in the ocean has long been observed. The effects of the more ubiquitous natural surface film caused by biological productivity are less established. The surface films damp surface short waves through surface tension, affecting microwave backscatter (e.g., Barger *et al.*, 1970; Alpers and Huhnerfuss, 1989). Such an effect has been widely inferred in synthetic aperture radar observations (e.g., Clemente-Colon and Yan, 1999; Lin *et al.*, 2001). But, since Huhnerfuss *et al.* (1978) measured such an effect by an airborne Ku-band scatterometer during the 1975 Joint North Sea Wave Project (JONSWAP 75) experiment, and Gade *et al.* (1998) performed a similar experiment, no clear effects of surface films on space-based scatterometer observations have been reported.

5.3 Atmospheric density stratification

The geophysical product of a scatterometer is the equivalent neutral wind (ENW), a theoretical parameter, because ENW is uniquely related to the surface stress measured by the scatterometer (Liu and Tang, 1996). The relation between ocean surface stress and actual wind at a reference height depends on atmospheric stability (density stratification). Liu (1984) found that the error (compared with collocated buoy measurements) of ENW from the Seasat scatterometer is a function of atmospheric stability, even after the effect of SST is removed. The error may be caused by residual stability effects that are not effectively removed in computing the ENW used in the calibration. The cause of error may also be that the maintenance of surface capillary waves depends on atmospheric stability, as suggested by Wu (1991).

5.4 Surface current

Wind stress depends on wind shear, or the difference between the wind vector at one level and the surface current; surface current has been included in the formulation of bulk parameterization of stress (e.g., Liu *et al.*, 1979). The importance of surface current feedback on the determination of stress in the tropical ocean was also studied by simulation using ocean general circulation models (e.g., Pacanowski, 1987). However, the ocean current is assumed to be negligible compared with wind in developing the wind retrieval algorithm. The effect of ocean surface current on the accuracy of scatterometer winds has been studied by Cornillon and Park (2001), Polito *et al.* (2001), and Kelly *et al.* (2001).

6. Weather and Marine Storm

Wind is air in motion. The most basic application of scatterometer wind measurement is in understanding atmospheric processes and predicting weather. Although the ERS-1 scatterometer was launched in 1991, the data were not operationally assimilated into NWP until 1994. All major weather forecast centers in Europe, Japan, and the U.S. started to implement the assimilation of ERS scatterometer winds between 1994 and 1997. NSCAT had only a short life span; the spacecraft failed before any NWP center could set up the system to assimilate its data. QuikSCAT has been in operation for two years, and the European Center for Medium Range Weather Forecast has just begun operational assimilation of the data. Besides the potential use in 4D assimilation by operational NWP, scatterometer data have been widely used by marine weather and hurricane centers in analyzing and predicting marine storms. The two major functions, NWP and tropical cyclone studies, are briefly described.

6.1 Impact on numerical weather forecast

While the scientific community was encouraged by the study of Cane *et al*. (1981), which suggested significant improvement in NWP using simulated scatterometer winds, a large number of impact studies on global models, performed later, using wind measured by the scatterometer on Seasat (e.g., Baker *et al*., 1984; Duffy *et al*., 1984; Yu and McPherson, 1984; Anderson *et al*., 1991; Ingleby and Bromely, 1991) did not find a large improvement in forecast results, although some improvements in analysis were found, particularly in the Southern Hemisphere. More significant impacts were found in regional experiments and over storms (e.g., Duffy and Atlas, 1986; Stoffelen and Cats, 1991). The errors in scatterometer geophysical model function, poor boundary layer parameterization in NWP models, and the failure to extend the influence of surface winds to upper levels, were possible obstacles that hampered any significant impact. The results of ERS impact studies were mixed. Stoffelen and Anderson (1997) found an improvement in analysis but not in forecast. Thepaut *et al*. (1993) and Andrew and Bell (1998) found a stronger positive impact. A comprehensive impact study of NSCAT data was preformed by Atlas *et al*. (1999), who revealed an approximately one-day extension of useful forecast skill in the Southern Hemisphere. Chang *et al*. (1999) showed that the assimilation of NSCAT data improves the numerical prediction of tropical mesoscale rainfall systems under the influence of the mountains in Taiwan. The improvement of the methodology whereby NSCAT and QuikSCAT data are assimilated into NWP model was discussed by Figa and Stoffelen (2000). Attempts to improve the description of mid-latitude marine storms through surface pressure fields generated from scatterometer winds have been successful (e.g., Levy and Brown, 1991; Brown and Zeng, 1994; Hsu and Wurtele, 1997; Zierden *et al*., 2000). Atlas *et al*. (2001) provided a review on scatterometer impact on NWP recently.

6.2 Study of tropical cyclones

During its short life span in the summer of 1978, the Seasat scatterometer did observe a large number of TC. Hawkins and Black (1983) validated the accuracy of wind retrieval at gale force (15–20 m/s). They were able to demonstrate that the advisory notices from hurricane centers consistently overestimate the radius of gale-force winds in TCs and wrongly portray the symmetry of the wind distribution, as compared with the scatterometer wind fields.

Using ERS-1 data, Hsu and Liu (1996) were able to derive the geostrophic winds and, subsequently, the pressure field from surface wind vectors measured by the ERS-1 scatterometer in Typhoon Oliver, using a boundary layer model and a gradient wind formula. The results contributed to the improved estimation of the intensity and the location of the storm. ERS data also allowed Liu and Chan (1999) to estimate the relative vorticity of TCs and compare the climatological sizes of Pacific and Atlantic TC. The positive impact in predicting and describing TCs by assimilating ERS scatterometer winds in NWP models was demonstrated in numerous studies (e.g., Tomassini *et al*., 1998; Le Marshall *et al*., 2000; Isaksen and Stoffelen, 2000).

NSCAT winds, together with water vapor measured by the Special Sensor Microwave/Imager (SSM/I) were used by Liu *et al*. (1997) to monitor Typhoon Tom, which started as a warm-core system, then merged with a mid-latitude low-pressure trough to form a large baroclinic storm. Chu *et al*. (1999) showed that NSCAT winds associated with Typhoon Ernie generated more realistic ocean responses (sea surface temperature, ocean current, and sea level changes) in an ocean general circulation model (OGCM) than winds from operational NWP winds in the South China Sea in the fall of 1996.

Liu *et al*. (2000a) showed that the surface wind and fresh water flux of the operational NWP model with the highest spatial resolution (Eta) could not resolve the rain bands of Hurricane Floyd. By simply replacing the surface level Eta wind divergence with QuikSCAT data, the fresh water flux computed from Eta data agree much better with observations by the rain radar on the Tropical Rain Measuring Mission (TRMM). The vertical profiles of heating and rain rate computed with QuikSCAT data revealed the eye and precipitation walls, in agreement with TRMM observations.

Katsaros *et al*. (2001) examined QuikSCAT data upstream of all the tropical cyclones in the Atlantic in the 1999 hurricane seasons, and found that, for the majority

of them, closed circulation with intensity meeting the criteria of a tropical depression were observed by QuikSCAT up to a few days before their identifications by the National Hurricane Center (NHC). NHC declared Floyd a tropical depression on September 7, 1999 east of the West Indies. QuikSCAT data were used to track the surface vortex all the way back to the African coast on September 2, 1999 (Liu, 2001). Because such vortices, in their early stages, are too small to be resolved by operational numerical weather prediction products, and have no clear cloud signal, the scatterometer, with its high spatial resolution, is the best means (if not the only means) to study these early vortices, their tracks across the Atlantic, and their evolution into full-blown hurricanes (Ritchie *et al.*, 2002). The role of scatterometers in the monitoring, understanding, and prediction of tropical cyclones has been well-recognized in the past decade (Veldon *et al.*, 2002).

7. Ocean-Atmosphere Interaction

The surface wind shear governs the momentum exchanges between the ocean and the atmosphere. Oceanographers, who were in great need of information on wind forcing of ocean circulation, were the first group to support space-based scatterometer missions. The classical application is to use scatterometer winds to force OGCM (Subsection 7.1). Since scatterometer winds have become continuously available, they have been used in studies of seasonal phenomena like the Monsoon (Subsection 7.2) and interannual signals like El Niño (Subsection 7.3). The high resolution allows studies of coastal jets and eddies (Subsection 7.4) and derivative parameters, such as atmospheric convergence (Subsection 7.5). The broad coverage reveals new phenomena in data-poor tropical (Subsection 7.6) and southern (Subsection 7.7) oceans. The unique contribution that scatterometer data can make to the estimation of turbulence fluxes of heat, moisture, and gases still needs to be developed (Subsection 7.8).

7.1 Forcing numerical ocean models

Scatterometers provide more realistic wind forcing with better spatial resolution in forcing ocean models (Liu *et al.*, 1998b). The response of OGCM to scatterometer wind forcing in tropical cyclones is discussed in Subsection 6.2 and under El Niño conditions in Subsection 7.3. Many studies show that wind fields derived from ERS scatterometers were superior to wind fields from NWP in simulating the ocean circulation with an OGCM (e.g., Fu and Chao, 1997; Grima *et al.*, 1999; Hackert *et al.*, 2001). The simulated upper ocean structure agrees better with measurements by buoys or sea levels measured by spaceborne altimeters. Barnier *et al.* (1994) studied the impact of the improved sampling of NSCAT over ERS-1, as wind forcing, on the simulation of the ocean circula-

tion in the Indian Ocean by an OGCM. Using NSCAT data, Chen *et al.* (1999a) demonstrated the sensitivity of tropical Pacific simulation to the temporal and spatial resolution of winds. Kelly *et al.* (1999) examined the predicted ocean response by a reduced-gravity, linear vorticity model and showed the greater skill of the NSCAT winds than ECMWF winds. Veschell *et al.* (1999) compared observed winds, NSCAT winds, and NSCAT stresses, and showed that NSCAT stresses simulated more realistic sea level changes. Milliff *et al.* (1999b) revealed the positive contribution of NSCAT winds in the study of ocean heat balance with OGCM. Yu and Moore (2000) examined the effect of possible rain-contaminated QuikSCAT winds in the ITCZ on the simulation of North Equatorial Counter Current.

7.2 Monsoon

Monsoons are the seasonal change of wind forced by the temperature contrast between the continent and the ocean. Liu and Xie (1999) computed the seasonal cycle of curl of wind stress (CWS) and sea level changes (SLC) over the South China Sea using six years of ERS scatterometer and Topex/Poseidon data. They show that the significant negative correlation between SLC and CWS in the central part of the basins is consistent with seasonal changes of Ekman pumping following the monsoons. In the deep basin, positive CWS causes upwelling, lower SLC, and cyclonic geostrophic current in winter, and negative CWS causes higher SLC and anticyclonic geostrophic current in summer.

The Somali Jet is closely linked to the Indian Monsoon. Halpern and Woiceshyn (1999) described the onset of the Jet, using observation from the NSCAT. They related the Jet to Indian rainfall, ocean Ekman pumping and decrease of the surface temperature of the Arabian Sea. Using both the wind vectors from QuikSCAT and rainfall from TRMM, Grodsky and Carton (2001) provided the first documentation of a biweekly oscillation in rainfall and wind that precedes the onset of monsoon season in the West Africa. Yeh *et al.* (2001) used QuikSCAT winds to study the Mei-yu front associated with the onset of the summer monsoon in East Asia.

7.3 El Niño

El Niño and Southern Oscillation (ENSO), the strongest interannual climatic signal, is believed to be associated with the collapse of the Pacific trade winds. Scatterometers have revealed, with unprecedented resolution, the evolution of the tropical wind systems associated with ENSO. Liu *et al.* (1995) related the westerly wind anomalies in the western Pacific observed by the ERS scatterometer to the propagation of Kelvin waves across the Pacific, as sea level changes observed by the Topex/Poseidon altimeter, and the subsequent ocean

warming and increase in atmospheric water vapor observed by spaceborne radiometers. Using ERS wind forcing, they were able to simulate the sea level and sea surface temperature changes using an OGCM.

Using wind measurements from NSCAT, Liu *et al.* (1998a) revealed that the westerly wind anomalies in the western Pacific at the start of the 1997 ENSO was connected to a northeastward flow of warm and moist air from the equatorial Pacific. This air stream moved past Hawaii, toward the west coast of the U.S. (it has been called the "Pineapple Express"). They postulated that the tropical air suppressed evaporative cooling and was associated with the anomalous warm water near the American west coast. The postulation was confirmed by the study of Brown and Fu (2000) who also used NSCAT data. The flow is part of the displaced cyclonic circulation, which shifts an ocean temperature dipole towards the coast; the dipole had been present in the North Pacific for almost a decade. This teleconnection hypothesis was supported in a long-term simulation (over 50 years) by the UCLA coupled ocean-atmosphere model (Yu *et al.*, 2000). Chen *et al.* (1999b) showed that using NSCAT winds for initialization has greatly improved the Lamont-Doherty Earth Observatory model forecasts of the 1997/1998 El Niño.

7.4 Coastal jets and eddies

Strong wind jets through the gaps of coastal mountains are known to excite strong response in the coastal oceans. Because of the narrow width, their structures are not well revealed either by operational NWP or *in situ* measurements. The improved spatial resolution of NSCAT helped to identify these wind jets. Kawamura and Wu (1998) used NSCAT data to demonstrate that the wind jet enhanced by the topographic effect around Vladivostok causes large turbulent heat flux, which in turn generates cold SST and a dense water mass, called the Japan Sea Proper Water. Bourassa *et al.* (1999) used NSCAT winds to examine the wind jet over the Gulf of Tehuantepec in Central America and its deflection by Hurricane Marco. The same jet was studied in detail by Chelton *et al.* (2000). The detailed wind forcing by QuikSCAT over this area, as shown in Fig. 2, provided sufficient spatial resolution to realistically simulate ocean upwelling in an OGCM and the consequent SST changes in the Gulf of Tehuantepec that agree with spaceborne observations (e.g., Liu *et al.*, 2001a).

When the normal winds from the northwest along the Southern California coast are stronger than normal, particularly during spring and summer, they interact with the local coastal topography to form an atmospheric cy-
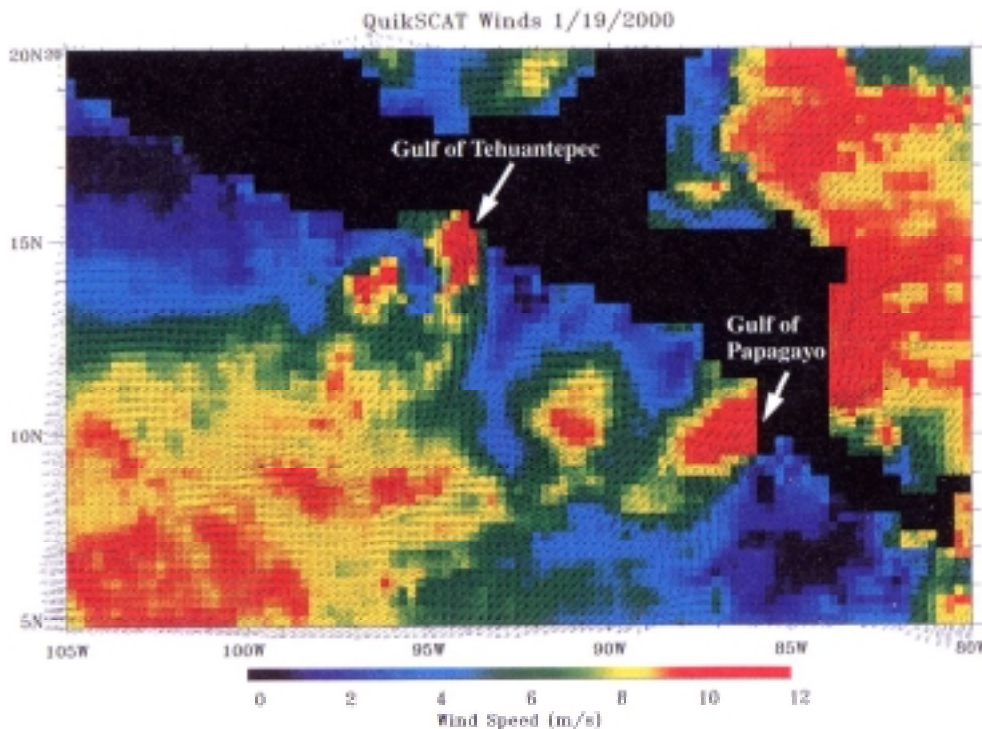

Fig. 2. Daily mean wind vectors superimposed on color image of wind speed derived from QuikSCAT measured by QuikSCAT showing wind jets through Central America.
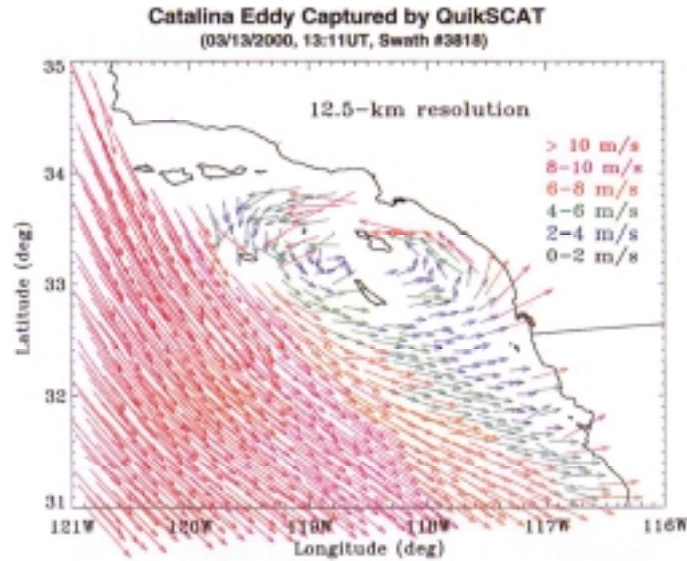
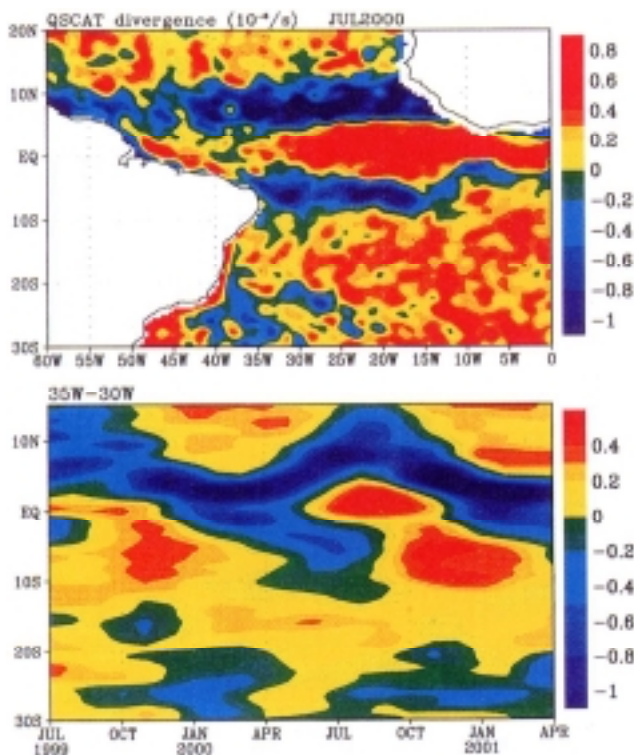Fig. 3. Catalina Eddy revealed by wind field derived from QuikSCAT.

Fig. 4. Map of ocean surface wind divergence for July 2000 (upper), and latitudinal-time variation of surface wind divergence averaged over 30°–35°W (lower), derived form QuikSCAT.

clonic vortex off Los Angeles, called the Catalina Eddy (Liu *et al*., 2001a). The gentle winds of the Eddy may direct the offshore marine layer toward the Los Angeles Basin, providing the cooling oceanic influence that is so welcome in this area. The Eddy is only 100–200 km in diameter; it is actually too small to appear in the present NWP models and is too shallow to have a strong influence on the cloud structure viewed by weather satellites. The high resolution (12.5 km) capability of QuikSCAT allows the visualization of the complete circulation of this "elusive" eddy (Fig. 3).

7.5 Convergence zone

The high quality and high resolution of scatterometer observations allow better representation of surface wind divergence. Using ERS-1 scatterometer data, Zheng *et al*. (1997b) described the variation of the Intertropical Convergence Zone (ITCZ), just north of the equator in the Pacific, the South Pacific Convergence Zone (SPCZ), running in an east-southeast direction from New Guinea. They also identified a convergence zone parallel to ITCZ, just south of the equator in the eastern Pacific (double ITCZ).

In the Atlantic, the QuikSCAT wind divergence clearly shows the ITCZ lying in an east-west direction, north of the equator, and South Atlantic Convergence Zone (SACZ) running southeast from the Brazilian coast at 20°S (Fig. 4). These features are well known. The new feature that QuikSCAT data reveal is the south ITCZ running eastward from the Recife, Brazil at 8°S, during the Austral winter. The convergence zone is collocated with
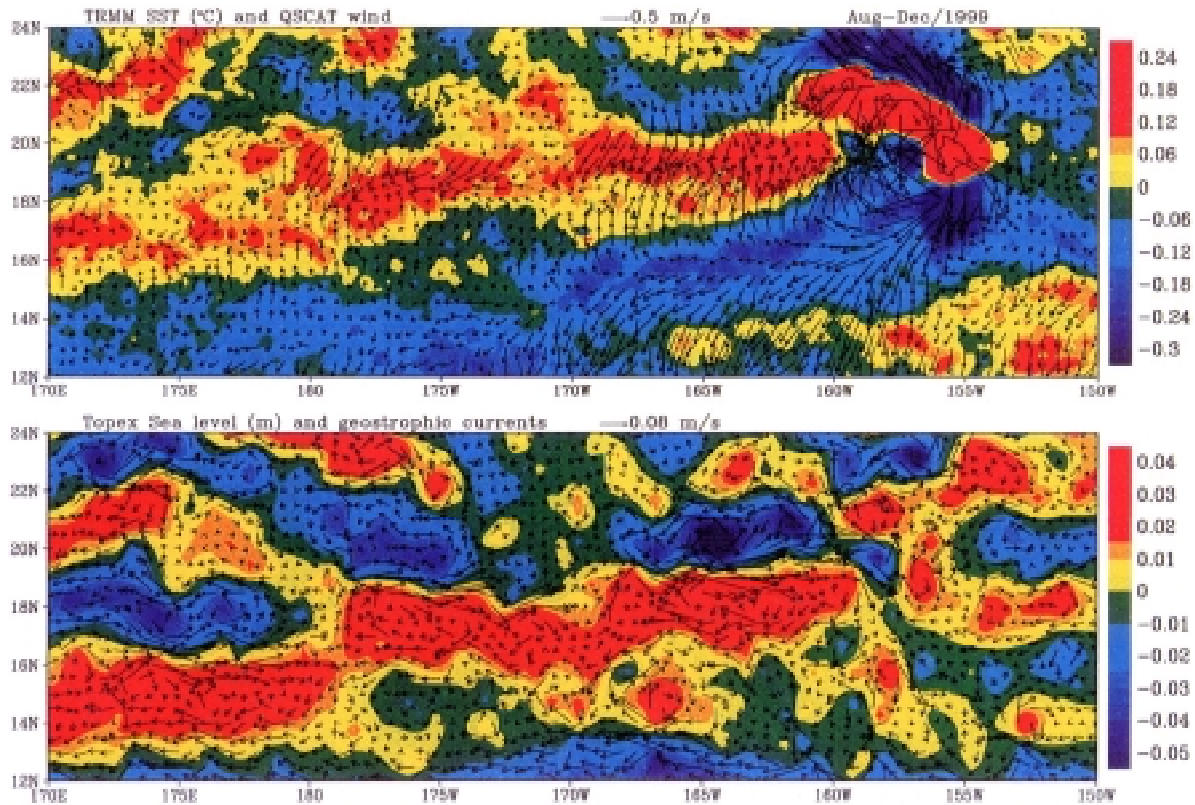
Fig. 5. Ocean surface wind vectors (arrows) derived from QuikSCAT superimposed on the map of sea surface temperature (color image) derived from TMI (upper). Changes of geostrophic currents (arrows) superimposed on sea level changes derived from Topex/Poseidon (lower). The meridional running-mean representing the large scale gradient has been removed from each set of data.

high SST and cloud liquid water, as observed by the TRMM Microwave Imager (TMI). Semyon Grodsky (personal communication, 2001) has also observed this convergence zone recently, using the same set of satellite data; there have been no other studies of this convergence zone. The time-latitude section in Fig. 4 shows that the three convergence zones in the Atlantic have different seasonal cycles. The ITCZ north of the equator has seasonal meridional migration. The ITCZ south of the equator is strong in winter (Austral) but almost disappears in summer, while the SACZ is strongest in the Austral summer.

7.6 New observations in tropical Pacific

The subtropical Pacific should be monotonous. The trade winds blow steadily from east to west, and so flows the North Equatorial Current. Only the Hawaiian Islands break this steady flow. After removing the large-scale meridional gradient, TMI reveals a warm water ridge stretching a few thousand kilometers from the Hawaii Islands to the western Pacific at 19°N (Fig. 5). The position of this warm water ridge coincides with the climatological-mean eastward current derived from eight

years of Lagrangian drifter data (Peter Niiler, personal communication, 2001). The Topex/Poseidon altimeter shows, in Fig. 5, bands of positive and negative sea level changes, implying cyclonic and anticyclonic current gyres with an eastward geostrophic current deviation between them at 19°N. The position of the positive zonal component of the geostropic current coincides with the position of the warm water. The warm water ridge is likely to be the result of advection from the western Pacific by a narrow eastward current. TMI also reveals a belt of high cloud liquid water overlying the warm water, probably as a result of atmospheric convection. The detailed wind fields provided by QuikSCAT reveals surface convergence and wind rotation (Fig. 5), which creates a zonal belt of positive wind stress curl. The wind forcing may provide a positive feedback to the eastward current. The eastward countercurrent and the wind patterns that stretch more than 3000 km east of Hawaii are likely to be triggered by the wind wake of the islands and sustained by positive ocean-atmosphere feedback. This narrow gap amid the westward flowing wind and current, which may have aided the ancient eastward migration of Polynesians

across half of the Pacific, had never been viewed a single system until QuikSCAT data were combined with two other microwave sensors by Xie *et al*. (2001) and Liu (2001).

The tropical instability waves (TIW) were best observed as meanders of the temperature front between the cold upwelling water of the Pacific equatorial cold tongue and the warm water to the north. Xie *et al*. (1998) first identified TIW in the wind variations observed by the ERS-1 scatterometer. The high-quality winds derived from QuikSCAT and coincident all weather SST measurements by TMI reveal the coherent propagation of atmospheric and oceanic parameters associated with TIW. The phase differences imply that the wind-SST coupling is caused by buoyancy instability and mixing in the atmospheric boundary layer, which has been confirmed by wind profiles measured on a research ship (Liu *et al*., 2000b). The analysis was extended to the south of the equator and to the Atlantic Ocean by Hashizume *et al*. (2001). Data from the scatterometer and the altimeter were also combined to study temperature advection in TIW by Polito *et al*. (2001). Chelton *et al*. (2001) provided further detailed analysis of the coupling of wind and SST in TIW.

7.7 Southern oceans

The deficiencies of NWP models, which are caused by a lack of knowledge and data, are most evident in the remote oceans around Antarctica. Here, scatterometer winds would have the strongest impact. NSCAT and QuikSCAT reveal three groups of intense storms surrounding Antarctica and they are associated with three maxima of sea ice extent (SIE) (Yuan *et al*., 1999; Liu, 2001). NSCAT observations have revealed positive feedback between wind pattern and the SIE maxima, and the SIE maxima provide favorable conditions for cyclogenesis in the open ocean. The quasi-stationary waves in the atmosphere around Antarctica were also examined by Milliff *et al*. (1999a), using NSCAT data. Using ERS-1 scatterometer and other space-based data, Gille *et al*. (2001) studied the relation between the transport by the Antarctic Circumpolar Current and wind forcing.

7.8 Turbulence flux

Wind shear facilitates the turbulent transfer of heat, moisture and gas between the ocean and the atmosphere. The transport is mostly parameterized in terms of wind speed (e.g., Liu *et al*., 1979; Liss and Merlivat, 1986). While scatterometer wind speed may improve the determination of the flux of carbon dioxide as demonstrated by Boutin *et al*. (1999), wind speed from other spacebased sensors, such as SSM/I and altimeters, can also be used. There are suggestions that the backscatter measured by the scatterometer contains information on secondary factors, such as small-scale wave fields, on ocean-atmos-

phere gas transfer, in additional to the information on wind speed. Wanninkhof and Bliven (1991) found an empirical relationship between backscatter and gas transfer in a wind tunnel. The additional advantage of using backscatter over using wind speed alone still has to be demonstrated in the open ocean with space-based observations.

The unique contribution of the scatterometer to the study of ocean-atmosphere exchanges is likely to be in estimating the transport terms in the conservation equation, whether it is the ocean biological pumping driven by the curl of wind stress or the atmospheric moisture advection in the hydrologic balance (e.g., Liu, 1993; Hsu *et al*., 1997).

8. Emerging Applications

From the vantage point of space, geophysical boundaries are not tall obstacles. The scatterometers measured backscatter from land and ice as well as from ocean. The geophysical interpretations of backscatter from land were more ambiguous but many new applications have recently emerged.

8.1 Flood index

Scatterometers are capable of monitoring not only the ocean winds, which feed moisture towards land, but the consequent flooding of the land. Both scattering and reflection from the surface contribute to the backscatter energy received by the scatterometer. Over dry land, scattering dominates and the horizontal polarization return (H) is less than the vertical polarization return (V). When the land gets flooded, however, the reflectivity of the surface increases greatly, and H becomes larger than V. The difference between reflectivity in H and V increases with incident angle, up to 80°. Over flooded land, the V/H ratio is less than 1 in the linear scale, or negative in the db scale. The opposite is true in the dry case.

QuikSCAT measures H at a constant incident angle of 54° over a swath of 1800 km and H at 46° over a 1400-km swath, providing a large difference in reflectivity. This is better suited to the monitoring of flooding than previous scatterometers, which had varying incidence angles. QuikSCAT data were used to depict the monsoons and tropical cyclones which brought excessive moisture into the Asian continent and to monitor the subsequent flooding over land, during summer and fall of 1999 (Liu *et al*., 2001b). The maps in Fig. 6 show that the flooding in the Yangtze Valley of China (30°N), represented by blue patches, is clearly visible in July, following strong summer monsoons. The flooding extent observed by QuikSCAT agrees with reports by the International Federation of the Red Cross. The flooding recedes in September, with the retreat of the summer monsoon and the advance of the winter monsoon. The intensity of the flood-
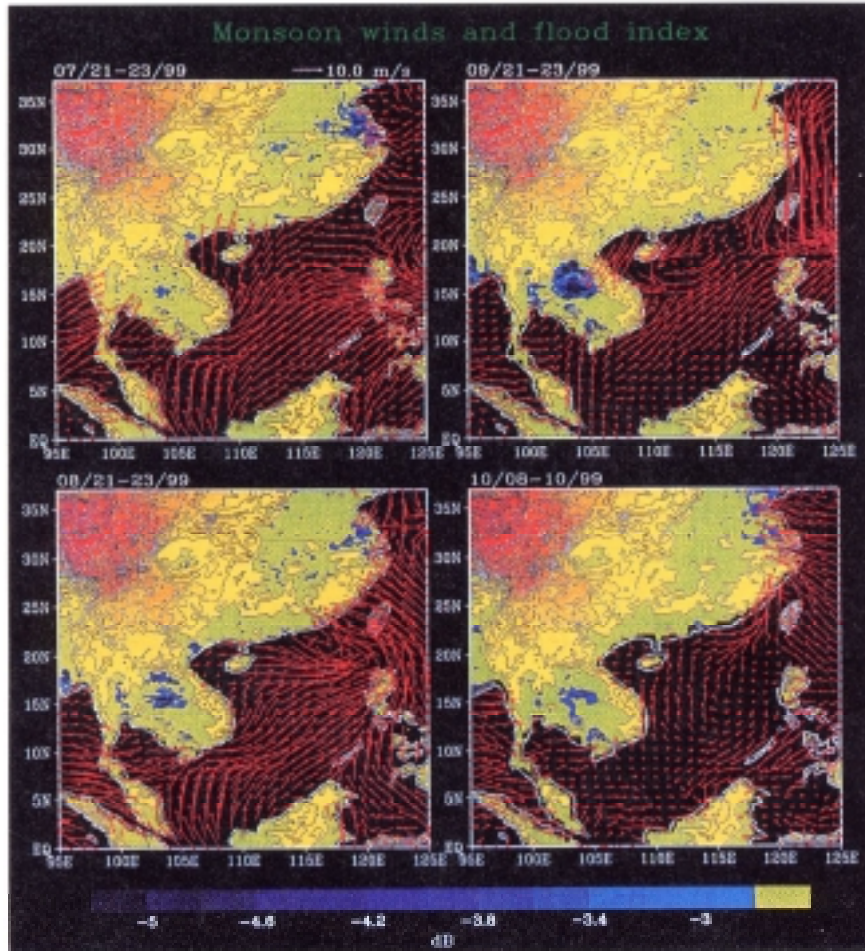
Fig. 6. Three-day average wind vectors over ocean and flood indexes over land derived from QuikSCAT observations, for four months in 1999. Topographic map for areas over 5-m elevation is plotted over flood indexes.

ing increases again in October, after the landfall of a typhoon.

8.2 Vegetation, soil moisture, snow cover, and freeze-thaw transition

Long and Hardin (1994) first showed that the backscatter observed by the scatterometer on Seasat, normalized to the same incident angle, and with enhanced spatial resolution, is highly correlated with the type of vegetation in the Amazon Basin. ERS scatterometer data were used by Wagner *et al.* (1999) to examine the effects of the seasonal changes of soil moisture on vegetation over the Iberian Peninsula. The same data set was used for regional mapping of soil moisture (Wagner, 2000; Woodhouse and Hoekman, 2000). Schmullius (1997) found a good correlation between ERS-1 observations and Siberian forest canopy; ERS-1 data were used to identify the freeze/thaw transition. Running *et al.* (1999) and Frolking *et al.* (1999) successfully monitored the transi-

tion of the boreal forest in Alaska from a frozen to a thawed condition using NSCAT. They related the observations to carbon flux dynamics. Wismann (2000) examined the freeze-thaw transition in Siberia between 1992 and 1999. Nghiem and Tsai (2001) demonstrated the sensitivity of NSCAT backscatter to snow conditions and the feasibility of monitoring global snow cover. Because the backscatter from land depends on surface roughness, vegetation, and soil moisture, a great deal of study is still required to distinguish the individual effects, if possible.

8.3 High-latitude studies

Scatterometer data have been used in three types of studies in the polar regions: sea-ice mapping, sea-ice dynamics, and change in the continental ice sheet. Yueh *et al.* (1997) developed a technique to discriminate between sea-ice and open ocean using scatterometer observations. The Arctic sea-ice extents observed by ERS, NSCAT, Radarsat, and SSM/I were compared in a number of stud-

ies (Yueh and Kwok, 1998; Ezraty and Cavanie, 1999). Kwok *et al.* (1999) studied the ice balance in the perennial ice zone of the Arctic Ocean, using NSCAT data. Remund and Long (1999) produced a detailed mapping of Antarctica using enhanced-resolution NSCAT data.

Liu, A. *et al.* (1998, 1999) used wavelet analysis of NSCAT backscatter to obtain daily sea-ice drift information. The ice motion derived from space-based data compared well with the existing array of Arctic Ocean buoys. Long and Drinkwater (1999), using the correlation between ice features detected by NSCAT, also computed ice motions in both the Arctic and the Antarctic.

Using Seasat scatterometer data with enhanced spatial resolution, Long and Drinkwater (1994) demonstrated a technique to monitor the firn line and the zones of various facies of snow and ice accumulation. Using ERS scatterometer and NSCAT data, Long and Drinkwater (1999) examined seasonal to decadal variations of Greenland ice zones, with an implication for climate change. Nghiem *et al.* (2001) made use of the high resolution and broad coverage of QuikSCAT to study snow-melt regions in Greenland. Their new approach does not require absolute calibration, which permits long-term monitoring of daily changes. Surface melting of Antarctica was also studied by Drinkwater and Liu (2000), using a combination of ERS scatterometer, Radarsat synthetic aperture radar, and SSM/I.

9. Future Mission and Technology

Quikscat will be followed by an identical scatterometer on board ADEOS-2, which is scheduled to be launched in 2002. If there is sufficient overlap between the operations of the two identical scatterometers, the importance of high frequency and high wave-number wind forcing on the ocean can be demonstrated (Milliff *et al.*, 2001). ESA is scheduling the launch of a series of C-band dual-swath advance scatterometers (ASCAT) on their operational platform METOP, starting in December 2005. NASA is planning to launch a polarimetric scatterometer on the Japanese Global Change Observation Mission (GCOM), so that two wide-swath scatterometers will provide continuous time series of high frequency wind forcing.

One of the drawbacks to scatterometry is the wind-direction ambiguity. The backscatter is a cosine function of the azimuth angle. In a recent experiment, it was demonstrated the correlation between copolarized and cross-polarized backscatter is a sine function of azimuth angle. Adding a cross polarizied backscatter receiver to the scatterometer on QuikSCAT can mitigate the directional ambiguity problem (Tsai *et al.*, 2000). Although QuikSCAT has a continuous scan, the azimuth angles are too close together at the outer swath and too far apart near nadir, hampering selection of wind direction. With polarimetric scatterometry we may achieve more uniform retrieval accuracy across the entire swath. Polarimetic scatterometry can separate rain effects in the atmosphere from those at the surface, and can perhaps improve the accuracy of retrieving wind under rain. A polarimetric scatterometer does not require a full circular scan to get the azimuth angles, and will ease accommodation problems on spacecraft. We are striving to infuse new technology so as to extend applications and to ease the transition into operational spacecraft, while preserving the continuity of high-quality wind-vector measurements.

10. Data Availability

Twice-daily maps of surface winds over global oceans, derived from objective interpolation of the observations by QuikSCAT, are displayed at http://airsea-www.jpl.nasa.gov. Digital data can be downloaded on line. Near-real-time scatterometer wind maps in swath format are displayed at http://manati.wwb.noaa.gov/quikscat. Standard NSCAT and QuikSCAT data can be requested through http://podaac.jpl.nasa.gov

References

Alpers, W. and H. Huhnerfuss (1989): The damping of ocean waves by surface films: a new look at an old problem. *J. Geophys. Res.*, **94**, 6251–6265.

Anderson, D., A. Hollingsworth, S. Uppala and P. Woiceshyn (1991): A study of the use of scatterometer data in the European Centre for Medium-range operational analysis-forecast model. 2. Data impact. *J. Geophys. Res.*, **96**, 2635–2647.

Andrew, P. L. and R. S. Bell (1998): Optimizing the United Kingdom Meteorological Office data assimilation for ERS-1 scatterometer winds. *Mon. Wea. Rev.*, **126**, 736–746.

Atlas, R., A. J. Busalacchi, E. Kalanay and S. Bloom (1987): Global surface wind and flux fields from model assimilation of SEASAT data. *J. Geophys. Res.*, **92**, 6477–6487.

Atlas, R., S. C. Bloom, R. N. Hoffman, E. Brin, J. Ardizzone, J. Terry, D. Bungato and J. C. Jusem (1999): Geophysical validation of NSCAT winds using atmospheric data and analyses. *J. Geophys. Res.*, **104**, 11,405–11,424.

Atlas, R., R. N. Hoffman, S. M. Leidner, J. Sienkiewicz, T.-W. Yu, S. C. Bloom, E. Brin, J. Ardizzone, J. Terry, D. Bungato and J. C. Jusem (2001): The effects of marine winds from scatteromemeter data on weather analysis and forecasting. *Bull. Amer. Meteor. Soc.*, **82**, 1965–1990.

Austin, S. and W. J. Pierson (1999): Mesoscale and synoptic-scale effect on the validation of NSCAT winds by means of data buoy reports. *J. Geophys. Res.*, **104**, 11,437–11,447.

Baker, W. E., R. Atlas, E. Kalnay, M. Halem, P. M. Woiceshyn, S. Peteherych and D. Edelmann (1984): Large-scale analysis and forecast experiments with wind data from the Seasat-A scatterometer. *J. Geophys. Res.*, **89**, 4927–4936.

Barger, W. R., W. D. Garrett, E. Mollo-Christensen and K. W. Ruggles (1970): Effects of an artificial slick upon the atmosphere and the ocean. *J. Appl. Meter.*, **9**, 396–400.

Barnier, B., J. Capella and J. O'Brien (1994): The use of satellite scatterometer winds to drive a primitive equation model of the Indian Ocean: the impact of bandlike sampling. *J. Geophys. Res.*, **99**, 14,187–14,196.

Bentamy, A., N. Grima and Y. Quilfen (1998): Validation of the gridded weekly and monthly wind fields calculated from ERS-1 scatterometer wind observations. *Global Atmos. Ocean System*, **6**, 373–396.

Bourassa, M. A., L. M. H. Freilich, D. M. Legler, W. T. Liu and J. J. O'Brien (1997): Wind observations from new satellite and research vessels agree. *Eos Trans., AGU*, **78**, 597, 602.

Bourassa, M. A., L. Zamudio and J. J. O'Brien (1999): Noninertial flow in NSCAT observations of Tehuantepec winds. *J. Geophys. Res.*, **104**, 11,311–11,319.

Boutin, J., J. Etcheto, M. Rafizadeh and D. C. E. Bakker (1999): Comparison of NSCAT, ERS 2 active microwave instrument, special sensor microwave imager, and carbon interface ocean atmosphere buoy wind speed: consequences for the air-sea CO_2 exchange coefficient. *J. Geophys. Res.*, **104**, 11,375–11,392.

Brown, R. A. (1982): Surface wind analyses for SEASAT. *J. Geophys. Res.*, **87**, 3355–3364.

Brown, R. A. (2000): On satellite scatterometer model functions. *J. Geophys. Res.*, **105**, 29,195–29,205.

Brown, R. A. and L. Zeng (1994): Estimating central pressures of the oceanic midlatitude cyclones. *J. Appl. Meter.*, **33**, 1088–1095.

Brown, R. G. and L.-L. Fu (2000): An examination of the spring 1997 mid-latitude east Pacific sea surface temperature anomaly. *Atmos.-Ocean*, **38**, 577–599.

Cane, M. A., V. J. Cardone, M. Halem and I. Halberstam (1981): On the sensitivity of numerical weather prediction to remotely sensed marine surface wind data: A simulation study. *J. Geophys. Res.*, **86**, 8093–8106.

Chang, C. P., S. C. Lin, C. S. Liou and W. T. Liu (1999): An experiment using NSCAT winds in the numerical prediction of tropical mesoscale rainfall systems under the influence of terrain. *Geophys. Res. Lett.*, **26**, 311–314.

Chelton, D. B., M. H. Freilich and S. K. Esbensen (2000): Satellite observations of the wind jets off the Pacific coast of Central America. Part I: Case studies and statistical characteristics. *Mon. Wea. Rev.*, **128**, 1993–2018.

Chelton, D. B., S. K. Esbensen, M. G. Schlax, N. Thum, M. H. Freilich, F. J. Wentz, C. L. Gentemann, M. J. McPhaden and P. S. Schoff (2001): Observations of coupling between surface wind stress and sea surface temperature in the eastern tropical Pacific. *J. Climate*, **14**, 1479–1498.

Chen, D., W. T. Liu, S. E. Zebiak, M. A. Cane, Y. Kushnir and D. Witter (1999a): The sensitivity of the tropical Pacific ocean simulation to the spatial and temporal resolution of wind forcing. *J. Geophys. Res.*, **104**, 11,261–11,271.

Chen, D., M. A. Cane and S. E. Zebiak (1999b): The impact of NSCAT winds on predicting the 1997/1998 El Niño: a case study with the Lamont-Dohderty Earth Obsevvatory model. *J. Geophys. Res.*, **104**, 11,321–11,327.

Chu, P. C., S. Lu and W. T. Liu (1999): Uncertainty of the South China Sea prediction using NSCAT and NCEP winds during tropical storm Ernie 1996. *J. Geophys. Res.*, **104**, 11,273–11,289.

Clemente-Colon, P. and X.-H. Yan (1999): Observations of east coast upwelling conditions in synthetic aperture radar imagery. *IEEE Trans. Geosci. Remote Sens.*, **37**, 2239–2248.

Cornillon, P. and K.-A. Park (2001): Warm core ring velocities inferred from NSCAT. *Geophys. Res. Lett.*, **28**, 575–578.

Donelan, M. A. and W. J. Pierson (1987): Radar scattering and equlibrium ranges in wind-generated waves with application to scatterometry. *J. Geophys. Res.*, **92**, 4971–5029.

Donnelly, W. J., J. R. Carswell, R. E. McIntosh, P. S. Chang, J. Wilkerson, F. Marks and P. G. Black (1999): Revised ocean backscatter models at C and Ku band under high-wind conditions. *J. Geophys. Res.*, **104**, 11,485–11,497.

Drinkwater, M. R. and X. Liu (2000): Seasonal to interannual variability in Antarctic sea-ice surface melt. *IEEE Trans. Geosci. Remote Sens.*, **38**, 1827–1842.

Duffy, D. G. and R. Atlas (1986): The impact of Seasat-A scatterometer data on the numerical predition of the Queen Elizabeth II storm. *J. Geophys. Res.*, **91**, 2241–2248.

Duffy, D. G., R. Atlas, T. Rosmond, E. Barker and R. Rosenberg (1984): The impact of Seaasat scatterometer winds on the navy's operational model. *J. Geophys. Res.*, **89**, 7238–7244.

Ebuchi, N. (1997): Sea surface temperature dependence of C-band radar cross sections observed by ERS-1/AMI scatterometer. *J. Adv. Mar. Sci. Tech. Soc.*, **3**, 157–168.

Ebuchi, N. (1999): Statistical distribution of wind speeds and directions globally observed by NSCAT. *J. Geophys. Res.*, **104**, 11,393–11,403.

Ebuchi, N. and H. C. Graber (1998): Directivity of wind vectors derived from the ERS-1/AMI scatterometer. *J. Geophys. Res.*, **103**, 7787–7798.

Ezraty, R. and A. Cavanie (1999): Construction and evaluation 12.5-km grid NSCAT backscatter maps over arctic sea ice. *IEEE Trans. Geosci. Remote Sens.*, **37**, 1685–1697.

Figa, J. and A. Stoffelen (2000): On the assimilation of Ku-band scatterometer winds for weather analysis and forecasting. *IEEE Trans. Geosci. Remote Sens.*, **38**, 1893–1902.

Freilich, M. H. (1986): Satellite scatterometer comparisons with surface measurements techniques and Seasat results. *Proc. Workshop ERS-1 Wind and Wave Calibration*, ESA SP-262, 57–62.

Freilich, M. H. and S. Dunbar (1993): A preliminary C-band scatterometer model function for the ERS 1 AMI instrument. *Proc. 1st ERS-1 Symposium*, ESA SP-359, 79–84.

Freilich, M. H. and S. Dunbar (1999): The accuracy of the NSCAT 1 vector winds: Comparisons with National Data Buoy Center buoys. *J. Geophys. Res.*, **104**, 11,231–11,246.

Frolking, S., K. C. McDonald, J. S. Kimball, J. B. Way, R. Ximmermann and S. W. Running (1999): Using the spaceborne NASA scatterometer (NSCAT) to determine the fro-

zen and thawed seasons. *J. Geophys. Res.*, **104**, 27,895–27,907.

Fu, L.-L. and Y. Chao (1997): The sensitivity of a global ocean model to wind forcing: a test using sea level and wind observations from satellites and operational wind analysis. *Geophys. Res. Lett.*, **24**, 1783–1786.

Gade, M., W. Alpers, H. Huhnerfuss, V. R. Wismann and P. A. Lange (1998): On the reduction of the radar backscatter by oceanic surface films: scatterometer measurements and their theoretical interpretation. *Remote Sens. Environ.*, **66**, 52–70.

Gille, S. T., D. P. Stevens, R. T. Tokmakian and K. J. Heywood (2001): Antarctic Circumpolar Current Response to Zonally-Averaged Winds. *J. Geophys. Res.*, **106**, 2743–2759.

Gonzales, A. E. and D. G. Long (1999): An assessment of NSCAT ambiguituy removal. *J. Geophys. Res.*, **104**, 11,449–11,457.

Grima, N., A. Bentamy, K. Katsaros and Y. Quilfen (1999): Sensitivity of an oceanic general circulation model forced by satellite wind stress fields. *J. Geophys. Res.*, **104**, 7967–7989.

Grodsky, S. A. and J. A. Carton (2001): Coupled land/atmosphere interactions in the West African Monsoon. *Geophys. Res. Lett.*, **28**, 1503–1506.

Hackert, E. C., A. J. Busalacchi and R. Murtugudde (2001): A wind comparison study using an ocean general circulatin model for the 1997–1998 El Niño. *J. Geophys. Res.*, **106**, 2345–2362.

Halpern, D. and P. M. Woiceshyn (1999): Onset of the Somali jet in the Arabian Sea during June 1997. *J. Geophys. Res.*, **104**, 18,041–18,046.

Hashizume, H., S.-P. Xie, W. T. Liu and K. Takeuchi (2001): Local and remote atmospheric response to tropical instability waves: a global view from space. *J. Geophys. Res.*, **106**, 10173–10185.

Hawkins, J. D. and P. G. Black (1983): SEASAT scatterometer detection of gale force winds near tropical cyclones. *J. Geophys. Res.*, **88**, 1674–1682.

Hoffman, R. N. (1982): SASS wind ambiguity removal by direct minimization. *Mon. Wea. Rev.*, **110**, 434–445.

Hsu, C. S. and W. T. Liu (1996): Wind and pressure fields near tropical cyclone Oliver derived from scatterometer observations. *J. Geophys. Res.*, **101**, 17,021–17,027.

Hsu, C. S. and M. G. Wurtele (1997): Construction of marine surface pressure fields from scatterometer winds. *J. Geophys. Res.*, **36**, 1249–1261.

Hsu, C. S., W. T. Liu and M. G. Wurtele (1997): Impact of scatteromometer winds on hydrologic forcing and convective heating through surface divergence. *Mon. Wea. Rev.*, **125**, 1556–1576.

Huhnerfuss, H., W. Alpers and W. L. Jones (1978): Measurements at 13.9 GHz of the radar backscattering cross section of the North Sea covered with an artificial surface film. *Radio Sci.*, **13**, 979–983.

Ingleby, N. B. and R. A. Bromley (1991): A diagnostic study of the impact of SEASAT scatterometer winds on numerical weather prediction. *Mon. Wea. Rev.*, **119**, 84–103.

Isaksen, L. and A. Stoffelen (2000): ERS scatterometer wind data impact on ECMWF's tropical cyclone forecasts. *IEEE Trans. Geosci. Remote Sens.*, **38**, 1885–1892.

Jones, W. L., F. J. Wentz and L. C. Schroeder (1978): Algorithm for inferring wind stress from SEASAT-A. *J. Spacecraft and Rockets*, **15**, 368–374.

Jones, W. L., L. C. Schroeder, D. H. Boggs, E. M. Bracalente, R. A. Brown, G. J. Dame, W. J. Pierson and F. J. Wentz (1982): The SEASAT-A satellite scatterometer: the geophyiscal evaluation of remotely sensed wind vectors over the ocean. *J. Geophys. Res.*, **87**, 3297–3317.

Jones, W. L., V. Cardone, W. J. Pierson, J. Zec, L. P. Rice, A. Cox and W. B. Sylvester (1999): NSCAT high-resolution surface wind measurements in Typhoon Violet. *J. Geophys. Res.*, **104**, 11,247–11,259.

Katsaros, K. B., E. B. Forde, P. Chang and W. T. Liu (2001): QuikSCAT facilitates early identification of tropical depressions in 1999 hurricane season. *Geophys. Res. Lett.*, **28**, 1043–1046.

Kawamura, H. and P. Wu (1998): Formation mechanism of Japan Sea Proper Water in the flux center off Vladivostok. *J. Geophys. Res.*, **103**, 21,611–21,622.

Kelly, K. A., S. Dickinson and Z. Yu (1999): NSCAT tropical wind stress maps: implications for improving ocean modeling. *J. Geophys. Res.*, **104**, 11,291–11,310.

Kelly, K. A., S. Dickensen, M. J. McPhaden and G. C. Johnson (2001): Ocean currents evident in satellite wind data. *Geophys. Res. Lett.*, **28**, 2469–2472.

Kwok, R., G. F. Cunningham and S. Yueh (1999): Area balance of the Arctic Ocean perennial ice zone: October 1996 to April 1997. *J. Geophys. Res.*, **104**, 25,747–25,759.

Le Marshall, J., L. Leslie, R. Morison, N. Pescod, R. Seecamp and C. Spinoso (2000): Recent developments in the continuous assimilation of satellite wind data for tropical cyclone track forcasting. *Adv. Space Res.*, **25**, 1077–1080.

Levy, G. and R. A. Brown (1991): Southern Hemisphere synoptic weather from satelllite scatterometer. *Mon. Wea. Rev.*, **119**, 2803–2813.

Lin, I.-I., L.-S. Wen, K.-K. Liu, W.-T. Tsai and A. K. Liu (2001): Evidence and quantification of the correlation between radar backscatter and ocean colour supported by simultaneously acquired *in situ* sea truth. *Geophys. Res. Lett.* (in press).

Liss, P. S. and L. Merlivat (1986): Air-sea gas exchange rates: Introduction and syntheis. p. 113–127. In *The Role of Air-Sea Exchange in Geochemical Cycling*, ed. by P. Buat-Menard, D. Reidel Publ. Co., Dordrecht.

Liu, A. K., Y. Zhao and W. T. Liu (1998): Sea ice motion derived from satellite agrees with buoy observations. *Eos Trans., AGU*, **79**, 353, 359.

Liu, A. K., Y. Xhao and S. Y. Wu (1999): Arctic sea ice drift from wavelet analysis of NSCAT and special sensor microwave imager data. *J. Geophys. Res.*, **104**, 11,529–11,538.

Liu, K. S. and J. C. L. Chan (1999): Size of tropical cyclones as inferred from ERS-1 and ERS-2 data. *Mon. Wea. Rev.*, **127**, 2992–3001.

Liu, W. T. (1984): The effects of the variations in sea surface temperature and atmospheric stability in the estimations of average wind speed by Seasat-SASS. *J. Phys. Oceanogr.*, **14**, 392–401.

Liu, W. T. (1993): Ocean surface evaporation. p. 265–278. In

Atlas of Satellite Observations Related to Global Change, ed. by R. J. Gurney, J. Foster and C. Parkinson, Cambridge University Press, Cambridge.

Liu, W. T. (2001): Wind over troubled water. *Backscatter*, **12**, No. 2, 10–14.

Liu, W. T. and W. G. Large (1981): Determination of surface stress by Seasat-SASS: A case study with JASIN Data. *J. Phys. Oceanogr.*, **11**, 1603–1611.

Liu, W. T. and W. Tang (1996): Equivalent Neutral Wind. JPL Pub. 96-17, Jet Propulsion Laboratory, Pasadena, 16 pp.

Liu, W. T. and X. Xie (1999): Spacebased observations of the oceanic responses to seasonal changes of south Asian monsoons. *Geophys. Res. Lett.*, **126**, 1473–1476.

Liu, W. T., K. B. Katsaros and J. A. Businger (1979): Bulk parameterization of air-sea exchanges in heat and water vapor including the molecular constraints at the interface. *J. Atmos. Sci.*, **36**, 1722–1735.

Liu, W. T., W. Tang and L. L. Fu (1995): Recent warming event in the Pacific may be an El Niño. *Eos Trans., AGU*, **76**, No. 43, 429–437.

Liu, W. T., W. Tang and R. S. Dunbar (1997): Scatterometer observes extratropical transition of Pacific typhoons. *Eos Trans., AGU*, **78**, 237, 240.

Liu, W. T., W. Tang and H. Hu (1998a): Spaceborne sensors observe various effects of anomalous winds on sea surface temperatures in the Pacific Ocean. *Eos Trans., AGU*, **79**, 249, 252.

Liu, W. T., W. Tang and P. S. Polito (1998b): NASA scatterometer provides global ocean-surface wind fields with more structures than numerical weather prediction. *Geophys. Res. Lett.*, **25**, 761–764.

Liu, W. T., H. Hu and S. Yueh (2000a): Interplay between wind and rain observed in Hurricane Floyd. *Eos. Trans., AGU*, **81**, 253, 257.

Liu, W. T., X. Xie, P. S. Polito, S. Xie and H. Hashizume (2000b): Atmosphere manifestation of tropical instability waves observed by QuikSCAT and Tropical Rain Measuring Missions. *Geophys. Res. Lett.*, **27**, 2545–2548.

Liu, W. T., H. Hu, Y. T. Song and W. Tang (2001a): Improvement of scatterometer wind vectors—impact on hurricane and coastal studies. *Proc. WCRP/SCOR Workshop of Airsea Flux Validation*, World Climate Research Programme, Geneva (in press).

Liu, W. T., X. Xie, W. Tang and S. V. Nghiem (2001b): Wind changes over the Western Pacific. *East Asia and Western Pacific Meteorology and Climate*. Vol. 4, World Scientific Co., London (in press).

Lleonart, G. T. and D. R. Blackman (1980): The spectral characteristics of wind-generated capillary waves. *J. Fluid Mech.*, **97**, 445–479.

Long, D. G. and M. R. Drinkwater (1994): Greenland ice-sheet properties observed by the Seasat-A scatterometer at enhanced resolution. *J. Glaciology*, **40**, 213–230.

Long, D. G. and M. R. Drinkwater (1999): Cryosphere application of NSCAT data. *IEEE Trans. Geosci. Remote Sens.*, **37**, 1671–1684.

Long, D. G. and P. J. Hardin (1994): Vegetation studies of the Amazon Basin using enhanced resolution Seasat scatterometer data. *IEEE Trans. Geosci. Remote Sen.*, **32**, 213–230.

Long, D. G., P. J. Hardin and P. T. Whiting (1993): Resolution enhancement of spaceborne scatterometer data. *IEEE Trans. Geosci. Remote Sens.*, **31**, 700–715.

Milliff, R. F., T. J. Hoar and H. van Loon (1999a): Quasi-stationary wave variability in NSCAT winds. *J. Geophys. Res.*, **104**, 11,425–11,435.

Milliff, R. F., W. G. Large, J. Morzel, G. Danabasoglu and T. M. Chin (1999b): Ocean general circulation model sensitivity to forcing from scatterometer winds. *J. Geophys. Res.*, **104**, 11,337–11,358.

Milliff, R. F., M. H. Freilich, W. T. Liu, R. Atlas and W. G. Large (2001): Global ocean surface vector wind observations from space. *Proc. Internation Conf. Ocean Observations for Climate Changes*, CSIRO Press (in press).

Moore, R. K. and A. K. Fung (1979): Radar determination of winds at sea. *Proc. IEEE*, **67**, 1504–1521.

Nghiem, S. V. and W.-Y. Tsai (2001): Global snow cover monitoring with spaceborne Ku-band scatterometer. *IEEE Trans. Geosci. Remote Sens.*, **39**, 2118–2134.

Nghiem, S. V., K. Steffen, R. Kwok and W.-Y. Tsai (2001): Detection of snow melt regions on the Greenland ice sheet using diurnal backscatter change. *J. Glaciology* (in press).

Pacanowski, R. C. (1987): Effect of equatorial currents on surface stress. *J. Phys. Oceanogr.*, **17**, 833–838.

Plant, W. J. (1986): A two-scale model of short wind-generated waves and scatterometry. *J. Geophys. Res.*, **91**, 10,735–10,749.

Plant, W. J. (2000): Effects of wind variability on scatterometry at low wind speeds. *J. Geophys. Res.*, **105**, 16,899–16,910.

Polito, P. S., J. P. Ryan, W. T. Liu and F. P. Chavez (2001): Oceanic and atmospheric anomalies of tropical instability waves. *Geophys. Res. Lett.*, **28**, 2233–2236.

Quilfen, Y., B. Chapron, T. Elfouhaily, K. Katsaros and J. Tournadre (1998): Observation of tropical cyclones by High-resolution scatterometry. *J. Geophys. Res.*, **103**, 7767–7786.

Remund, Q. P. and D. G. Long (1999): Sea ice extent mapping using Ku band scatterometer data. *J. Geophys. Res.*, **104**, 11,515–11,527.

Ritchie, E., J. Simpson, W. T. Liu, C. Veldon, K. Brueske and J. Halvorsen (2002): A closer look at hurricane formation and intensification using new technology. In *Coping with Hurricanes. Chapter 12*, ed. by R. Simpson, M. Garstang and R. Anthes, Amer. Geophys. Union (in press).

Running, S. W., J. B. Way, K. C. McDonald, J. S. Kimball, S. Frlking, A. R. Keyser and R. Zimmerman (1999): Radar remote sensing proposed for monitoring freeze-thaw transitions in boreal regions. *Eos Trans., AGU*, **80**, 213.

Schmullius, C. C. (1997): Monitoring Siberian forest and agriculture with the ERS-1 wind scatterometer. *IEEE Trans. Geosci. Remote Sens.*, **35**, 1364–1366.

Schroeder, L. C., D. H. Boggs, G. Dome, I. M. Halberstam, W. L. Jones, W. J. Pierson and F. J. Wentz (1982): The relationship between wind vector and normalized radar cross section used to derive SEASAT-A satellite sctererometer winds. *J. Geophys. Res.*, **87**, 3318–3336.

Shaffer, S. J., R. S. Dunbar, S. V. Hsiao and D. G. Long (1991): A median-filer-based ambiguity removal algorithm for NSCAT. *IEEE Trans. Geosci. Remote Sens.*, **29**, 167–174.

Spencer, M. W., C. Wu and D. G. Long (2000): Improved resolution backscatter measurements with the SeaWinds pencil-beam scatterometer. *IEEE Trans. Geosci. Remote Sens.*, **38**, 89–104.

Stoffelen, A. and D. Anderson (1997): Scatterometer data interpretation: Estimation and validation of the transfer function CMOD4. *J. Geophys. Res.*, **102**, 5767–5780.

Stoffelen, A. and G. J. Cats (1991): The impact of Seasat-A scatterometer data on high-resolution analysis and forecasts: The development of the QEII storm. *Mon. Wea. Rev.*, **119**, 2794–2802.

Thepaut, J.-N., R. N. Hoffman and P. Coutier (1993): Interactions of dynamics and observations in a four-dimensional variational assimilation. *Mon. Wea. Rev.*, **121**, 3393–3414.

Thiria, S., C. Mejia, F. Badran and M. Crepon (1993): A neural network approach for modeling nonlinear transfer functions: Application for wind retrieval from spaceborne scatterometer data. *J. Geophys. Res.*, **98**, 22,827–22,841.

Tomassini, M., D. LeMeur and R. W. Saunders (1998): Near-surface satellite wind observations of Hurricanes and their impact on ECMWF model analyses and forecasts. *Mon. Wea. Rev.*, **126**, 1274–1286.

Tsai, W.-Y., S. Nghiem, J. Huddelstgon, M. Spencer, B. Stiles and R. West (2000): Polarimetric scatteromometer: a promising technique for improving ocean surface measurements from space. *IEEE Trans. Geosci. Remote Sens.*, **38**, 1903–1921.

Veldon, C., K. Bruske, C. Kummerow, W. T. Liu, J. Simpson, S. Braun and R. Anthes (2002): The burgeoning role of weather satellites. In *Coping with Hurricanes. Chapter 11*, ed. by R. Simpson, M. Garstang and R. Anthes, Amer. Geophys. Union (in press).

Verschell, M. A., M. A. Bourassa, D. E. Weissman and J. J. O'Brien (1999): Ocean model validation of the NASA scatterometer winds. *J. Geophys. Res.*, **104**, 11,359–11,373.

Wagner, W. (2000): Large-scale soil moisture mapping in western Africa using the ERS scatterometer. *IEEE Trans. Geosci. Remote Sens.*, **38**, 1777–1782.

Wagner, W., G. Lemoine, M. Borgeaud and H. Rott (1999): A study of vegetation cover on ERS scatterometer data. *IEEE Trans. Geosci. Remote Sens.*, **37**, 938–948.

Wanninkhof, R. H. and L. F. Bliven (1991): Relationship between gas exchange, wind speed, and radar backscatter in a large wind-wave tank. *J. Geophys. Res.*, **96**, 2785–2786.

Weissman, D. E. and H. C. Graber (1999): Satellite scatterometer studies of ocean surface stress and drag coefficients using a direct model. *J. Geophys. Res.*, **104**, 11,329–11,335.

Wentz, F. J. and D. K. Smith (1999): A model function for the ocean-normalized radar cross-section at 14 GHz derived from NSCAT observations. *J. Geophys. Res.*, **104**, 11,449–11,514.

Wentz, F. J., D. Smith and C. Mears (2001): Advanced algorithm for QuikSCAT and SeaWinds/AMSR. *Proc. of IGARSS 2001*, IEEE (in press).

Wismann, V. (2000): Monitoring of seasonal thawing in Siberia with ERS scatterometer data. *IEEE Trans. Geosci. Remote Sens.*, **38**, 1804–1809.

Woodhouse, I. H. and D. H. Hoekman (2000): A model-based determination of soil moisture trends in Spain with the ERS-scatterometer. *IEEE Trans. Geosci. Remote Sens.*, **38**, 1783–1793.

Wright, J. W. (1968): A new model for sea clutter. *IEEE Trans. Antennas and Prop.*, **AP-16**, 217.

Wu, J. (1991): Effects of atmospheric stability on ocean ripples: a comparison between optical and microwave measurements. *J. Geophys. Res.*, **96**, 7265–7269.

Wurtele, M. G., P. M. Woiceshyn, S. Peterherych, M. Borowski and W. S. Appleby (1982): Wind direction alias removal studies of SEASAT scatterometer-derived wind fields. *J. Geophys. Res.*, **87**, 3365–3377.

Xie, S. P., M. Ishiwagtari, H. Hashizumi and K. Takeuchi (1998): Coupled ocean-atmosphere waves on the equatorial front. *Geophys. Res. Lett.*, **25**, 3863–2966.

Xie, S. P., W. T. Liu, Q. Liu and M. Nonaka (2001): Far-reaching effects of the Hawaiian Island on the Pacific Ocean-Atmosphere. *Science*, **292**, 2057–2060.

Yeh, H.-C., T.-J. G. Chen and W. T. Liu (2001): Kinematic characteristics of a Meiyu Front detected by the QuikSCAT oceanic winds. *Mon. Wea. Rev.* (in press).

Yu, J. Y., W. T. Liu and C. R. Mechoso (2000): The SST anomaly Dipole In the northern subtropical Pacific and its relationship with ENSO. *Geophys. Res. Lett.*, **27**, 1931–1934.

Yu, T. W. and R. D. McPherson (1984): Global data assimilation experiment with scatterometer winds from SEASAT-A. *Mon. Wea. Rev.*, **112**, 368–376.

Yu, Z. and D. W. Moore (2000): Validating the NSCAT winds in the vicinity of the Pacific Intertropical Convergence Zone. *Geophys. Res. Lett.*, **27**, 2121–2124.

Yuan, X., D. G. Martinson and W. T. Liu (1999): The effect of air-sea-ice interaction on winter 1996 southern ocean subpolar storm distribution. *J. Geophys. Res.*, **104**, 1991–2007.

Yueh, S. H. and R. Kwok (1998): Arctic sea ice extent and melt onset from NSCAT observations. *Geophys. Res. Lett.*, **25**, 4369–4372.

Yueh, S. H., R. Kwok, S. Lou and W. Tsai (1997): Sea ice identification using dual-polarized Ku-band scatterometer data. *IEEE Trans. Geosci. Remote Sens.*, **35**, 560–569.

Yueh, S. H., R. West, F. K. Li, W. Y. Tsai and R. Lay (2000): Dual-polarized Ku-band backscatter signatures of hurricane ocean winds. *IEEE Trans. Geosci. Remote Sens.*, **38**, 73–88.

Yueh, S. H., B. Stiles, W.-Y. Tsai, H. Hu and W. T. Liu (2001): QuikSCAT geophysical model function for tropical cyclones and application to Hurricane Floyd. *IEEE Trans. Geosci. Remote Sens.* (in press).

Zheng, Q., X.-H. Yan, N. E. Huang, V. Klemas and J. Pan (1997a): The effects of water temperature on radar scattering from the ocean surface. *Global Atmosphere and Ocean System*, **5**, 273–294.

Zheng, Q., X. H. Yan, W. T. Liu, W. Tang and D. Kurz (1997b): Seasonal and interannual variability of atmospheric convergence zones in the tropical Pacific observed with ERS-1 scatterometer. *Geophys. Res. Lett.*, **24**, 261–263.

Zierden, D. F., M. A. Bourassa and J. J. O'Brien (2000): Cyclone surface pressure fields and frontogenesis from NASA Scatterometer (NSCAT) winds. *J. Geophys. Res.*, **105**, 23,967–23,981.